Journal of Inflammation Research

Dovepress
Taylor & Francis Group

Open Access Full Text Article

ORIGINAL RESEARCH

Chronic Exposure to Cigarette Smoke Induces Pyroptosis in Pulmonary Epithelial Cells via EGR1/USP44/TRAF6 Axis in COPD

Chaofan Cao[1,2], Zhaoshuang Zhong[3], Bo Wu[4], Bo Zou[5], Hui Jia[3], Jiahuan Xu[3], Guixian Xiao[2], Shuyue Xia[1,3]

[1]Graduate School of Dalian Medical University, Dalian Medical University, Dalian, Liaoning, People's Republic of China; [2]Department of Respiratory Medicine, The Second Affiliated Hospital of Shenyang Medical College, Shenyang, Liaoning, People's Republic of China; [3]Department of Respiratory Medicine, Central Hospital Affiliated to Shenyang Medical College, Shenyang, Liaoning, People's Republic of China; [4]Department of Thoracic Surgery, Cancer Hospital of China Medical University, Liaoning Cancer Hospital & Institute, Shenyang, Liaoning, People's Republic of China; [5]Department of Respiratory Medicine, The Fourth Affiliated Hospital of China Medical University, Shenyang, Liaoning, People's Republic of China

Correspondence: Guixian Xiao; Shuyue Xia, Email 18002453148@163.com; syx262@126.com

Background: Chronic obstructive pulmonary disease (COPD) is characterized by a persistent, progressive, and irreversible decline in lung function, primarily driven by persistent airway obstruction and pulmonary inflammation. Cigarette smoking is a major risk factor, as tobacco smoke harms pulmonary epithelial cells, frequently inducing chronic inflammation and ultimately resulting in structural lung lesions. Although pyroptosis is a well-recognized mechanism implicated in cigarette smoke extract (CSE)-induced lung epithelial damage, the specific regulatory roles of early growth response 1 (EGR1) and ubiquitin-specific peptidase 44 (USP44) in this process remain to be fully elucidated. Since inhibiting pyroptosis represents a promising therapeutic strategy for COPD, clarification of the roles of these factors is critically important.

Methods: We used a well-established cigarette smoke exposure protocol to establish COPD cellular and animal models. We assessed the extent of pyroptosis in the cellular model using techniques including propidium iodide (PI) staining, Annexin V/PI flow cytometry, and Western blot analysis for cleaved caspase-1 and gasdermin D (GSDMD), identified the pivotal downstream gene EGR1 through transcriptome sequencing, and validated the function of the EGR1/USP44/TNF receptor-associated factor 6 (TRAF6) axis in the model. In the animal model, we observed the therapeutic effect of USP44 knockdown on COPD progression.

Results: EGR1 was identified as a key response gene in CSE-stimulated lung epithelial cells. Moreover, our findings indicated that EGR1 plays a crucial role in facilitating CSE-induced pyroptosis. EGR1 transcriptionally enhances the expression of USP44, which subsequently facilitates the deubiquitination and stabilization of TRAF6, thus promoting pyroptosis in lung epithelial cells. The inhibition of either EGR1 or USP44 markedly reduced CSE-induced pyroptosis, underscoring their critical roles in this pathological process. Knocking down USP44 in animal models effectively alleviated COPD-like pathological changes caused by cigarette smoke exposure.

Conclusion: We identified the EGR1/USP44/TRAF6 signaling axis implicated in the pyroptosis of lung epithelial cells induced by CSE, indicating that this axis has the potential to serve as a therapeutic target for the treatment of smoking-induced COPD.

Keywords: COPD, cigarette smoke, pyroptosis, EGR1, USP44, TRAF6

Introduction

It is estimated that chronic obstructive pulmonary disease (COPD) is responsible for more than three million deaths annually, and this figure is expected to continue increasing. COPD is currently the third leading cause of death worldwide.[1] The defining characteristic of COPD is persistent airflow obstruction caused by airway irregularities and/or alveolar structural degradation, which ultimately leads to chronic respiratory symptoms.[2] Smoking continues to be a major risk factor for COPD.[3] Exposure to cigarette smoke (CS) damages pulmonary epithelial cells through multiple mechanisms, thereby contributing to the progressive development of COPD. One key mechanism is the CS-induced

Received: 13 June 2025
Accepted: 19 November 2025
Published: 27 November 2025

protease-antiprotease imbalance. This imbalance is initiated when CS prompts epithelial cells to release chemokines, which recruit immune cells such as macrophages, lymphocytes, and neutrophils. These immune cells then secrete proteases that degrade the extracellular matrix, ultimately causing airway remodeling and alveolar structural damage.[4,5] Furthermore, CS-induced disruption of the oxidant-antioxidant balance further exacerbates COPD progression.[6] CS exposure induces oxidative stress, leading to pulmonary epithelial cell damage and the activation of various forms of cell death, including necrosis, pyroptosis, apoptosis, and ferroptosis.[7,8]

Pyroptosis is an inflammatory type of programmed cell death that is triggered by pathogen invasion or cellular damage. It is primarily mediated by caspase-1 and is typically activated through inflammasomes, such as the NOD-like receptor family pyrin domain containing 3 (NLRP3). Exposure to CS has been shown to induce pyroptosis in pulmonary epithelial cells to varying degrees. Specifically, CS upregulates the expression and promotes the activation of NLRP3, which subsequently recruits and cleaves the caspase-1 precursor into its active form. Activated caspase-1 cleaves gasdermin D (GSDMD), producing a pore-forming N-terminal domain that executes pyroptotic cell death. Caspase-1 additionally processes the proforms of interleukin-1β (IL-1β) and interleukin-18 (IL-18) into their mature forms and facilitates their secretion, thereby amplifying the inflammatory response.[9] Furthermore, CS can upregulate TNF receptor-associated factor 6 (TRAF6), which in turn exacerbates pyroptosis. TRAF6, a pivotal member of the TRAF protein family, plays a crucial role in acute inflammatory responses by transducing signals through multiple pathways.[10,11] TRAF6 serves as a pivotal adaptor protein linking upstream Toll-like receptors (TLRs) to the downstream NLRP3 inflammasome, and it plays a crucial role in activating caspase-1-dependent pyroptosis in pulmonary epithelial cells.[12,13] Thus, targeting TRAF6 for inhibition has emerged as a promising therapeutic strategy to mitigate pyroptosis and potentially alleviate CS-induced COPD.[14] However, the regulatory mechanisms governing TRAF6 protein stability in response to CS exposure remain poorly understood.

Ubiquitination is a critical post-translational modification that regulates protein stability and function. Dysregulation of the balance between ubiquitination and deubiquitination is frequently observed in numerous diseases and plays a crucial role in the regulation of cell death pathways.[15] Ubiquitinated proteins are typically targeted for degradation via the proteasome system, a process that can be reversed by deubiquitinating enzymes.[16] TRAF6 can undergo diverse types of ubiquitination and deubiquitination modifications. However, the precise effects of CS-induced ubiquitination on TRAF6 remain poorly understood. Consequently, elucidating this process is key to understanding the mechanism of pyroptosis in COPD. Notably, the expression and activity of deubiquitinating enzymes are frequently subject to precise regulation by transcription factors. Early growth response 1 (EGR1) is a zinc-finger transcription factor that is rapidly induced by external stimuli, including CS. It acts as a pivotal mediator of cellular responses to environmental stress. EGR1 regulates the expression of downstream target genes involved in inflammatory responses and in various cell fate decisions, including pyroptosis.[17,18] However, whether EGR1 modulates TRAF6-mediated pyroptosis by regulating specific deubiquitinating enzymes remains unreported.

This study identified ubiquitin-specific peptidase 44 (USP44) as an essential deubiquitinating enzyme for TRAF6, whose expression is transcriptionally regulated by EGR1. USP44-mediated deubiquitination enhances TRAF6 protein stability, thereby promoting CS-induced pyroptosis in pulmonary epithelial cells. We propose that CS induces pyroptosis via the EGR1/USP44/TRAF6 axis, thereby contributing to the pathogenesis of COPD.

Materials and Methods

Cell Culture

A549, Beas-2B, and HEK-293T cell lines were procured from Procell, China. A549 cells were cultivated in Dulbecco's Modified Eagle Medium (DMEM) /F12 (PM150312, Procell, China) enriched with 10% fetal bovine serum (FBS; 164210, Procell, China) and 1% penicillin/streptomycin (P/S; PB180120, Procell, China). Beas-2B and HEK-293T cells were cultivated in DMEM (PM150210, Procell, China) enriched with 10% FBS and 1% P/S. All cells were sustained at 37 °C in 5% CO_2.

Cigarette Smoke Extract (CSE)

Unfiltered Honghe cigarettes (11 mg tar, 1.0 mg nicotine, 12 mg carbon monoxide per cigarette) were lit. Using a syringe pump, mainstream cigarette smoke was aspirated into a syringe at a constant rate of 8 mL/s. Subsequently, 10 mL of serum-free medium pre-warmed to 37°C was forcefully injected into the tube, allowing the smoke to bubble thoroughly through the medium, with the entire smoking process lasting 5 minutes. The resulting CSE solution was first calibrated to pH 7.4, then standardized and quality-controlled by measuring optical density at 320 nm (OD_{320}) and 540 nm (OD_{540}), only CSE batches with a ΔOD (OD_{320} - OD_{540}) ranging from 0.9 to 1.2 were used for experiments. After sterilization through a 0.22 μm filter (Merck, Germany), the standardized solution was designated as 100% CSE, which was then diluted to specified concentrations in serum-free medium and used within 30 minutes of preparation.

Cell Viability Assay

The Cell Counting Kit-8 (CCK-8; C0037, Beyotime, China) was used to assess cell viability. At a density of 5×10^3 cells per well, A549 and Beas-2B cells from different experimental groups were inoculated into 96-well plates. The cells were then incubated for 48 hours at 37°C with 5% CO_2 under varying concentrations of CSE (0%, 2.5%, 5%, and 10%).The plates were then incubated for two more hours after adding 10 μL of CCK-8 reagent to each well. At 450 nm, absorbance was measured with a microplate reader.

Lactate Dehydrogenase (LDH) Assay

Using an LDH Cytotoxicity Assay Kit (C0016, Beyotime, China) and following the instructions provided by the manufacturer, we determined the amount of LDH that was released in the supernatants of the cell culture. One hundred microliters of supernatant was collected from each group for analysis.

Cell Pyroptosis Assay

Propidium iodide (PI) staining was used to measure pyroptosis. After being inoculated into 6-well plates at a density of 2.5×10^5 cells per well, A549 and Beas-2B cells were incubated for 48 hours at 37°C with 5% CO_2 under varying concentrations of CSE (0%, 2.5%, 5%, and 10%). Cells were then stained with PI solution (2 μg/mL), and pictures were taken with a fluorescence microscope (NIB900, Nexcope, China) in both red fluorescence and bright field settings. The proportion of PI-positive cells, signifying pyroptosis, was measured utilizing ImageJ software (NIH, USA).

Flow Cytometry Analysis

Pyroptosis was evaluated utilizing an Annexin V-FITC/PI Detection Kit (C1062S, Beyotime, China). PI-positive cells were deemed pyroptotic. After inoculating A549 and Beas-2B cells into 6-well plates at a density of 2.5×10^5 cells/well, the cells were incubated for 48 hours at 37°C with 5% CO_2 under varying concentrations of CSE (0%, 2.5%, 5%, and 10%).Subsequent to incubation, cells were collected, rinsed twice with PBS, and stained in accordance with the manufacturer's guidelines. Following a 15-minute incubation at ambient temperature in the absence of light, stained cells were examined using a FACSVerse flow cytometer (BD, USA). Data were obtained and analyzed utilizing FlowJo software (BD, USA).

Transmission Electron Microscopy

After being fixed for 24 hours in 2.5% glutaraldehyde, cells were post-fixed for 3 hours in 1% osmium tetroxide. Samples were dehydrated using a series of graded ethanol concentrations (50%, 70%, 90%, and 100%, each for 10 minutes), embedded in resin, and then cut into 50–60 nm slices. A transmission electron microscope (HT7700, Hitachi, Japan) was used to examine the sections after they had been stained with uranyl acetate and lead citrate.

Western Blot

RIPA buffer enhanced with protease inhibitors (GRF101, Epizyme, China) was used to lyse cells or tissues. Following SDS-PAGE fractionation, equal amounts of protein (30 μg for both cell lysates and tissue homogenates) were loaded per

lane and electrophoretically transferred to PVDF membranes (WJ002, Epizyme, China). Membranes were incubated with 5% non-fat milk for two hours at room temperature before being incubated with primary and secondary antibodies. A Tanon 5200 system was used to identify the signals, and ImageJ was used to measure the band intensities. The following antibodies were used: NLRP3, Caspase1, GSDMD, P-like endoplasmic reticulum kinase (PERK), p-PERK, Eukaryotic translation initiation factor 2α (eIF2α), p-eIF2α, Activation transcription factor 4 (ATF4), EGR1, USP44, TRAF6, and β-Actin. Detailed information including catalog numbers and dilutions was made available in Supplementary Table 1.

Enzyme-Linked Immunoassay (ELISA)

Using ELISA Kits (both purchased from Beyotime, China) and following the instructions provided by the manufacturer, we quantified the concentrations of IL-1β and IL-18 in the cell culture supernatants separately.

RNA Sequence and Data Analysis

RNA sequencing (RNA-seq) and data analysis were performed with three biological replicates. For RNA isolation, 5×10^6 cells per replicate were used, and total RNA was extracted using the TaKaRa MiniBEST Universal RNA Extraction Kit (Code No. 9796). RNA was purified by poly-A selection for mRNA enrichment. RNA-seq library construction and sequencing were outsourced to BGI (Shenzhen, China), with 10× sequencing depth and 6 Gb of raw data per sample. Biological replicates were independent, using cells from different passages/batches and three separate experiments. Differentially expressed genes (DEGs) were identified using the DESeq2 package (R language), with significance defined as a false discovery rate (FDR) < 0.05 and absolute $\log_2$(fold change) > 1.

Plasmids

All plasmids were obtained from Miaoling Plasmids, China. The complete list of plasmids was provided in Supplementary Table 2.

Luciferase Reporter Assay

Hek-293T cells were inoculated in 24-well plates using the Luciferase reporter assay. Using Lipo 3000, the luciferase reporter plasmid, Renilla expression plasmid, and specific plasmids were co-transfected into the corresponding cells. After 48 hours of transfection, cells were lysed. Using the Dual-Luciferase Reporter Assay System (E1910, Promega, USA), the activities of firefly luciferase and Renilla luciferase were measured.

Chromatin Immunoprecipitation (ChIP) Assay

Following the manufacturer's instructions, ChIP experiments were carried out using the ChIP Kit (Bes5001, BersinBio, China). To cross-link proteins and DNA, A549 cells were fixed in culture medium containing 1% formaldehyde for ten minutes at room temperature. To break down DNA to a size range of 200–500 bp, cells were lysed and then incubated with 0.5 μL of micrococcal nuclease for 20 minutes at 37°C. The mixture was then immunoprecipitated at 4°C overnight using either a negative control IgG or 2.5 μg of EGR1 antibody (4153, CST, USA). The purified DNA was amplified using qRT-PCR with primers designed as outlined follow: USP44 forward primer 5′-TGCGGCGGCTACGACAGC −3′, reverse primer 5′-GCGGCCACCGGCAGGTT −3′. qRT-PCR was performed by TB Green® *Premix Ex Taq*™ II (Tli RNaseH Plus)(RR820A,TAKARA,Japan).

Co-Immunoprecipitation (Co-IP)

After collection, the cells were lysed for 30 minutes on ice using Passive Cell Lysis Buffer containing protease inhibitors. Each sample's supernatant was mixed with an antibody, with the corresponding IgG serving as a negative control. After gently rotating the mixture for four hours, it was rinsed three times using 1× lysis/binding/wash buffer. Agarose-protein A/G beads (YJ201, Epizyme, China) were added after overnight gentle agitation at 4°C, and then incubated for an additional 4 hours at room temperature. Western blotting was used for analysis after samples were incubated at 98°C for 15 minutes to elute bound proteins using 2× SDS-PAGE loading buffer.

Poly-Ubiquitination Detection Assay

HEK-293T cells were co-transfected with Myc-USP44, Flag-TRAF6, and His-ubiquitin plasmids to evaluate USP44-mediated TRAF6 ubiquitination. Co-IP was conducted 48 hours post-transfection, and the levels of TRAF6 and ubiquitin were assessed by Western blot analysis. The antibodies used were as follows: Anti-Myc-tag (60003-2-Ig, Proteintech, China), Anti-Flag-tag (20543-1-AP, Proteintech, China), and Anti-His-tag (66005-1-Ig, Proteintech, China).

Animal Model

Eight-week-old male C57BL/6J mice were randomly allocated into four groups (n = 5 per group): Control, Cigarette Smoke (CS), sh-USP44, and CS + sh-USP44. For the sh-USP44 and CS + sh-USP44 groups, USP44 knockdown was achieved via intratracheal instillation of lentivirus carrying mouse USP44-shRNA (vector: pLV3-U6-USP44 (mouse)-shRNA-CopGFP-Puro), using the Lipofectamine™ 3000 Transfection Kit (Thermo Fisher Scientific, Cat. No.: L3000075). All mice were exposed to room air; the CS-exposed groups (CS, CS + sh-USP44) received Honghe cigarette smoke in a chamber (3 h/day: 12 cigarettes/45 min, 4 sessions/day) for 5 days/week over 6 months. Body weight was monitored weekly. After the final exposure, mice were euthanized by cervical dislocation following intraperitoneal injection of pentobarbital (150 mg/kg). Lung tissues were collected, with analyses focusing on the alveolar region. The study was approved by the Ethics Committee of the Cancer Hospital of China Medical University (Approval No.: GZR202403118) and conducted according to relevant guidelines.

Immunohistochemistry

Tissues were first fixed in formalin and then embedded in paraffin. Four-micron-thick sections were mounted on glass slides, deparaffinized with xylene, and rehydrated with graded ethanol. Slides were immersed in 10 mM sodium citrate and boiled for 30 minutes for antigen retrieval. After blocking for 1 hour, sections were incubated overnight at 4°C with primary antibodies: anti-EGR1 (55117-1-AP, Proteintech, China, 1:100), anti-USP44 (YT4841, Immunoway, China, 1:100), and anti-TRAF6 (YM8516, Immunoway, China, 1:100). Following PBS washes, sections were incubated with horseradish peroxidase (HRP)-conjugated secondary antibody for 1 hour at room temperature, then visualized with 3,3′-diaminobenzidine (DAB). Staining intensity was graded as: 0 (negative; no positive staining), 1 (weakly positive; light yellow), 2 (positive; brownish yellow), and 3 (strongly positive; dark brown). The proportion of positive cells was graded as: 1 (≤25%), 2 (26–50%), 3 (51–75%), and 4 (>75%). The final score was the product of these two grades.

Statistical Analysis

GraphPad Prism 8.0 was used to conduct all statistical analyses. For comparisons between two groups, the Student's *t*-test was applied. For comparisons among multiple groups, one-way ANOVA was performed, followed by Tukey's post-hoc test to determine pairwise differences. P-values < 0.05 were considered statistically significant. Data are presented as mean ± standard deviation (SD), and each experiment was repeated at least three times.

Results

CSE Induces Pyroptosis in Pulmonary Epithelial Cells

To determine whether CSE induces pyroptosis in pulmonary epithelial cells, A549 and Beas-2B cells were treated with increasing concentrations of CSE, and multiple pyroptosis markers were assessed 48 hours after treatment. CCK-8 assay results showed that CSE significantly decreased the viability of A549 and Beas-2B cells. Consistent with this, LDH assay results showed that CSE treatment induced cytotoxic damage to these cells (Figure 1A). To confirm pyroptosis induction, the percentage of PI-positive cells in A549 and Beas-2B populations was evaluated through PI staining and flow cytometry. PI-positive cells, indicating impaired membrane integrity, were considered indicative of pyroptosis. Both methods consistently demonstrated that CSE significantly increased the proportion of PI-positive cells, particularly at concentrations of 5% and 10% (Figure 1B and C). Next, we used transmission electron microscopy to observe morphological changes in the cells before and after treatment with 10% CSE. Cells treated with 10% CSE exhibited distinct pyroptotic features, including a large number of pyroptotic bodies, varying degrees of cellular swelling, and

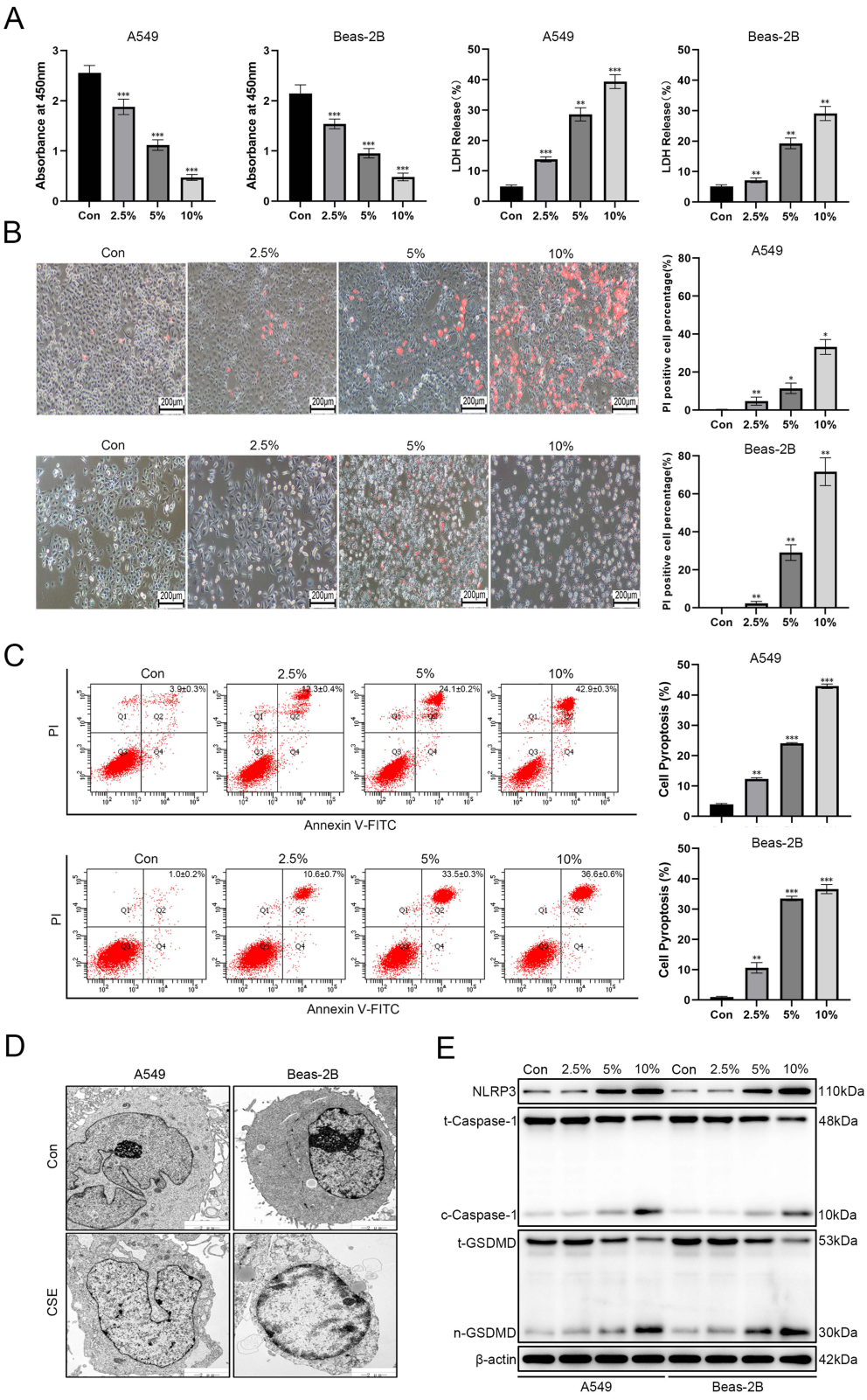

Figure 1 CSE Induces Pyroptosis in Pulmonary Epithelial Cells. (**A**) The CCK-8 assay was employed to evaluate the impact of CSE exposure on cell viability in A549 and Beas-2B cells, whereas the LDH assay assessed CSE-induced cytotoxicity in these cells; (**B**) PI staining was conducted to ascertain the percentage of pyroptotic cells subsequent to CSE induction in A549 and Beas-2B cells; (**C**) Flow cytometry was employed to quantify pyroptotic cell populations following CSE treatment in A549 and Beas-2B cells; (**D**) Transmission electron microscopy was used to examine the morphological and ultrastructural alterations caused by CSE in A549 and Beas-2B cells; (**E**) Western blot analysis was employed to identify alterations in the expression of proteins associated with the NLRP3/Caspase-1/GSDMD signaling pathway subsequent to CSE induction in A549 and Beas-2B cells. *$P < 0.05$, **$P < 0.01$, ***$P < 0.001$.

impaired membrane integrity (Figure 1D). Finally, we assessed the activation of the canonical pyroptosis pathway, which includes NLRP3, Caspase-1, and GSDMD. Western blot analysis showed that CSE treatment increased the protein levels of NLRP3, cleaved Caspase-1 (c-Caspase-1), and the N-terminal fragment of GSDMD (n-GSDMD) (Figure 1E). Densitometric quantification further confirmed the concentration-dependent upregulation of these pyroptosis-related proteins (Supplementary Figures 1 and 2). Furthermore, ELISA confirmed that CSE stimulation significantly and dose-dependently increased the release of IL-1β and IL-18 into the cell culture supernatant (Supplementary Figure 3). Collectively, these findings demonstrate that CSE induces pyroptosis in pulmonary epithelial cells in a concentration-dependent manner.

CSE induction activates the PERK/eIF2α/ATF4 signaling pathway, leading to the upregulation of EGR1 expression levels

To clarify the molecular mechanism underlying CSE-induced pyroptosis in lung epithelial cells, we performed transcriptome sequencing to detect gene expression changes in Beas-2B cells following induction with 5% or 10% CSE (Figure 2A). Next, we identified the intersection of genes upregulated following induction with 5% and 10% CSE to obtain a set of candidate genes (Figure 2B). This approach aimed to narrow the candidate gene range by identifying differentially expressed genes that exhibited a dose-dependent response to CSE. The identified candidate genes showed a strong correlation with endoplasmic reticulum (ER) stress and included the following genes (ordered by log_2FC values): CYP1A1, EGR1, TIPARP, NIBAN1, BEX2, AQP3, GGT4P, ENSG00000234261, NPTX1, IQCN, ATF3, CYP1B1, STC2, GDF15, ANXA10, EPGN, DDIT3, ENSG00000285133. We next confirmed the activation of the ER stress-related PERK/eIF2α/ATF4 signaling pathway and analyzed the expression of EGR1, a prominent differentially expressed gene, in both A549 and Beas-2B cells following CSE treatment via Western blotting. The results confirmed that CSE activated the PERK/eIF2α/ATF4 pathway and enhanced EGR1 protein expression (Figure 2C), indicating that CSE may facilitate pyroptosis through the PERK/eIF2α/ATF4/EGR1 axis.

Knockdown of EGR1 Attenuates the CSE-Induced Pyroptosis Response in Pulmonary Epithelial Cells

To test this hypothesis, we transfected A549 and Beas-2B cells with EGR1-shRNA to silence EGR1 expression and investigated whether this intervention could attenuate CSE-induced pyroptosis in these cells. The CCK-8 assay results showed that EGR1 knockdown attenuated the CSE-induced reduction in cell viability. Similarly, LDH assay results showed that EGR1 knockdown reduced CSE-induced cytotoxicity (Figure 3A). PI staining combined with flow cytometry confirmed that EGR1 knockdown decreased the percentage of PI-positive cells following CSE treatment (Figure 3B and C). Western blot analysis showed that EGR1 knockdown inhibited the CSE-induced upregulation of NLRP3, c-Caspase-1, and n-GSDMD (Figure 3D). Furthermore, ELISA confirmed that EGR1 knockdown significantly attenuated the CSE-induced release of IL-1β and IL-18 into the cell culture supernatant (Supplementary Figure 4). Collectively, these data demonstrate that inhibition of EGR1 attenuates CSE-induced pyroptosis in pulmonary epithelial cells.

The Transcription Factor EGR1 Promotes the Expression of USP44

To investigate the downstream mechanisms by which EGR1 modulates CSE-induced pyroptosis, we analyzed our transcriptomic data for genes associated with ubiquitination and deubiquitination. Using a screening threshold of $log_2FC > 1$ and $P < 0.01$, USP44 was the only gene that met these criteria ($log_2FC = 1.043$, $P < 0.01$). We subsequently obtained the promoter sequence of USP44 (from −2000 bp to +100 bp) from the Eukaryotic Promoter Database (EPD) and utilized the JASPAR database (https://jaspar.elixir.no/) to predict EGR1 binding sites on this promoter. To experimentally validate the transcriptional regulation of USP44 by EGR1, we performed dual-luciferase reporter assays and CHIP combined with quantitative PCR (ChIP-qPCR). The dual-luciferase reporter assay showed that EGR1 significantly enhanced USP44 promoter activity (Figure 4A). Additionally, ChIP-qPCR analysis confirmed that EGR1 directly binds to the USP44 promoter region (Figure 4B).

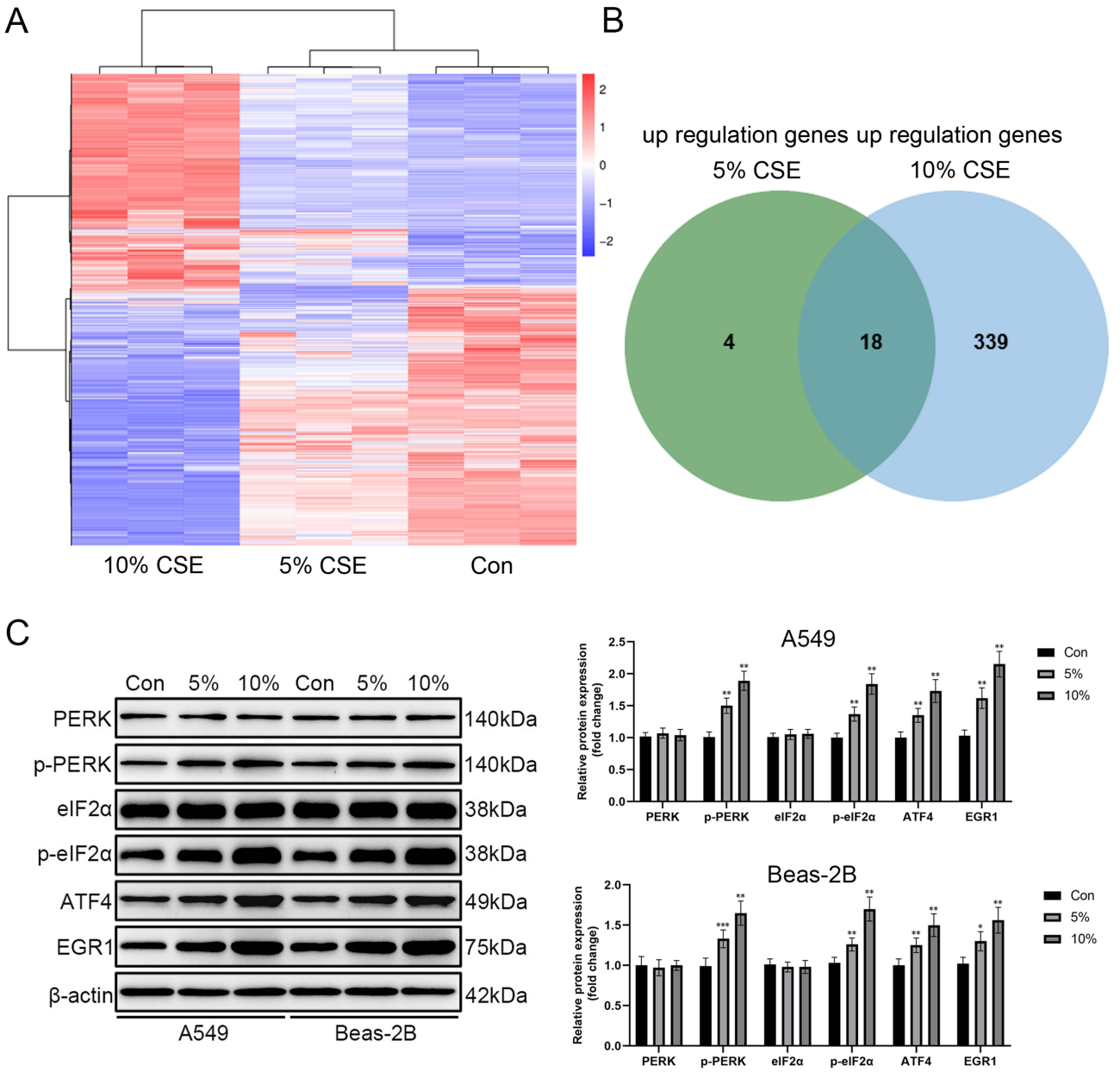

Figure 2 CSE Induction Activates the PERK/eIF2α/ATF4 Signaling Pathway to Enhance EGR1 Expression. (**A**) RNA-Seq analysis was performed to investigate alterations in gene expression in Beas-2B cells following CSE treatment, with the findings shown as a heatmap; (**B**) Venn diagram depicting shared upregulated genes subsequent to 5% and 10% CSE exposure; (**C**) Western blot analysis was employed to identify alterations in the expression of proteins associated with the ER stress-related PERK/eIF2α/ATF4 signaling pathway and EGR1 protein subsequent to CSE induction in A549 and Beas-2B cells. *$P < 0.05$, **$P < 0.01$, ***$P < 0.001$.

Knockdown of USP44 Attenuates the CSE-Induced Pyroptosis Response in Pulmonary Epithelial Cells

To investigate the role of USP44 in CSE-induced pyroptosis, we transfected A549 and Beas-2B cells with USP44-specific shRNA to achieve USP44 knockdown. This approach allowed us to assess whether knockdown of USP44 could attenuate CSE-induced pyroptosis. The CCK-8 assay results showed that USP44 knockdown significantly attenuated the CSE-induced reduction in cell viability. Similarly, LDH assay results showed that USP44 knockdown attenuated CSE-induced cellular injury (Figure 5A). PI staining combined with flow cytometry showed that USP44 knockdown inhibited the CSE-induced increase in the percentage of PI-positive cells (Figure 5B and C). Western blot analysis confirmed that USP44 knockdown mitigated the CSE-induced upregulation of pyroptosis-associated proteins, namely NLRP3,

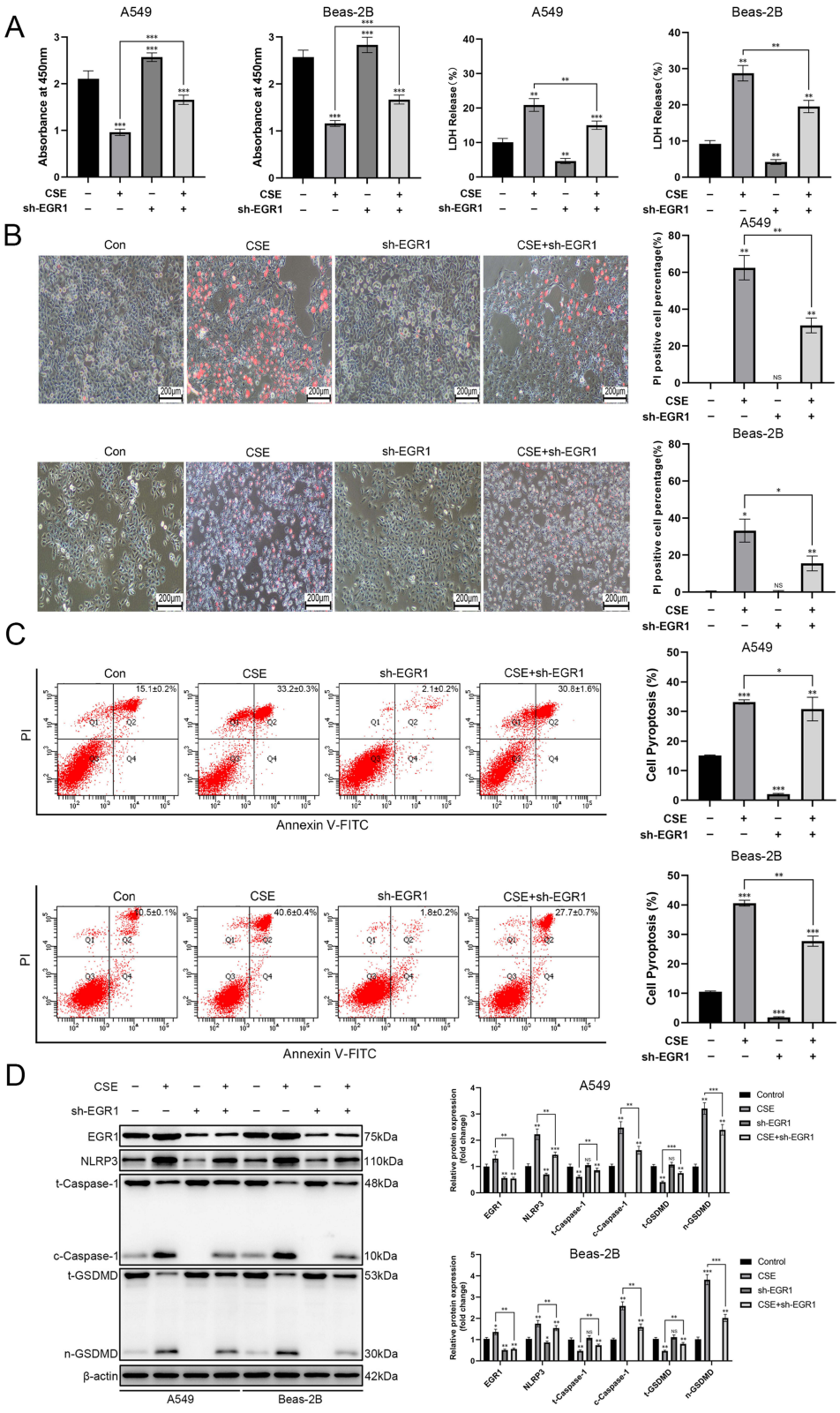

Figure 3 EGR1 Knockdown Mitigates CSE-Induced Pyroptosis in Pulmonary Epithelial Cells. (**A**) CCK-8 and LDH assays were employed to assess the impact of EGR1 knockdown on CSE-induced decreases in cell viability and increases in cellular damage, respectively; (**B**) The effect of EGR1 knockdown on CSE-induced pyroptosis was evaluated using propidium iodide staining; (**C**) Flow cytometry was used to quantify the percentage of pyroptotic cells following EGR1 knockdown in CSE-treated cells; (**D**) Western blot analysis was used to assess the expression of proteins in the NLRP3/Caspase-1/GSDMD pathway following EGR1 knockdown in CSE-treated cells.*$P < 0.05$, **$P < 0.01$, ***$P < 0.001$.

https://doi.org/10.2147/JIR.S546865

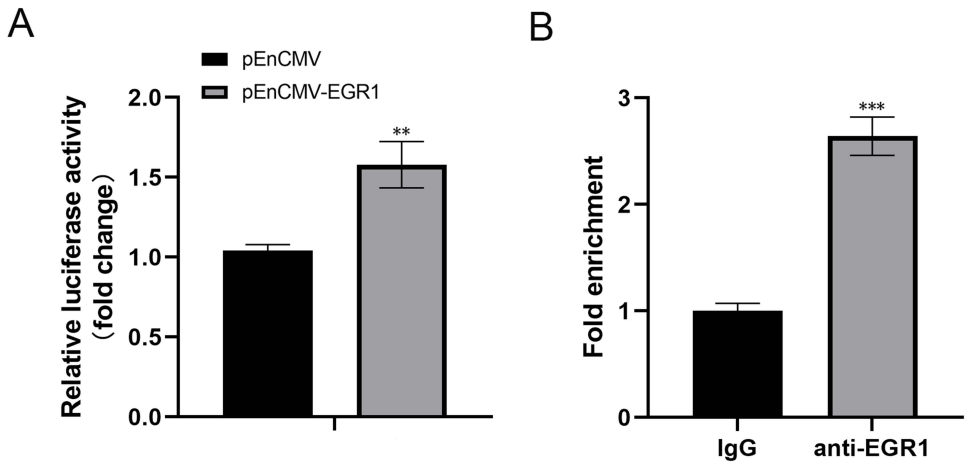

Figure 4 The Transcription Factor EGR1 Promotes USP44 Expression. (**A**) A dual-luciferase reporter assay was employed to examine the influence of EGR1 on USP44 promoter activity; (**B**) ChIP-qPCR analysis was conducted to validate the binding interaction between EGR1 and the USP44 promoter region. ***P* < 0.01, ****P* < 0.001.

c-Caspase-1, and n-GSDMD (Figure 5D). Furthermore, ELISA confirmed that USP44 knockdown significantly attenuated the CSE-induced release of IL-1β and IL-18 into the cell culture supernatant (Supplementary Figure 5). Collectively, these findings demonstrate that USP44 knockdown significantly suppresses CSE-induced pyroptosis in pulmonary epithelial cells.

USP44 Enhances the Stability of TRAF6 Protein

We used the UbiBrowser 2.0 platform (http://ubibrowser.ncpsb.org.cn) to predict potential deubiquitination substrates of USP44. Among the candidates associated with pyroptosis, TRAF6 had the highest ranking (confidence score = 0.843). To determine whether USP44 enhances TRAF6 protein stability via deubiquitination, we first treated A549 and Beas-2B cells with cycloheximide (CHX) to inhibit protein synthesis and then assessed the effect of USP44 knockdown on the half-life of TRAF6 protein. Western blot analysis showed that USP44 knockdown reduced the half-life of TRAF6 protein, thereby decreasing its stability (Figure 6A). Next, to assess the degradation of TRAF6 via the proteasome pathway, we treated the cells with MG132, a proteasome inhibitor. The results showed that USP44 knockdown decreased TRAF6 protein levels, and these levels were restored by MG132 treatment (Figure 6B), suggesting that USP44 protects TRAF6 from proteasomal degradation. Co-IP assays confirmed a direct physical interaction between USP44 and TRAF6 (Figure 6C). To evaluate the functional significance of this interaction, we investigated the effect of USP44 overexpression on TRAF6 ubiquitination. Ubiquitination immunoprecipitation assays showed that USP44 overexpression significantly decreased the level of TRAF6 ubiquitination (Figure 6D); specifically, it reduced K48-linked ubiquitination while having minimal effect on K63-linked ubiquitination (Figure 6E). Using the PhosphoSitePlus® PTM database (https://www.phosphosite.org/), we identified potential ubiquitination sites on TRAF6, namely K104, K124, K331, K356, and K489. Subsequently, we constructed TRAF6 plasmids with site-directed mutations (K104R, K124R, K331R, K356R, and K489R) and assessed the effect of USP44 on these variants. The ubiquitination immunoprecipitation assays demonstrated that USP44 obstructs TRAF6 ubiquitination at various sites, specifically K124 and K331 (Figure 6F).

Knockdown of USP44 Ameliorates Pathological Changes in a Mouse Model of CS-Induced COPD

To validate the cellular findings in vivo, we established a CS-induced COPD murine model. USP44 knockdown was achieved via intratracheal administration of a lentivirus carrying USP44-specific shRNA into mouse lungs. Histopathological analysis revealed that, compared to control mice, CS-induced mice exhibited significant alveolar wall destruction and varying degrees of bullae-like pathological changes. USP44 knockdown significantly ameliorated these pathological changes (Figure 7A). CS exposure resulted in the upregulation of EGR1, USP44, and TRAF6 in lung

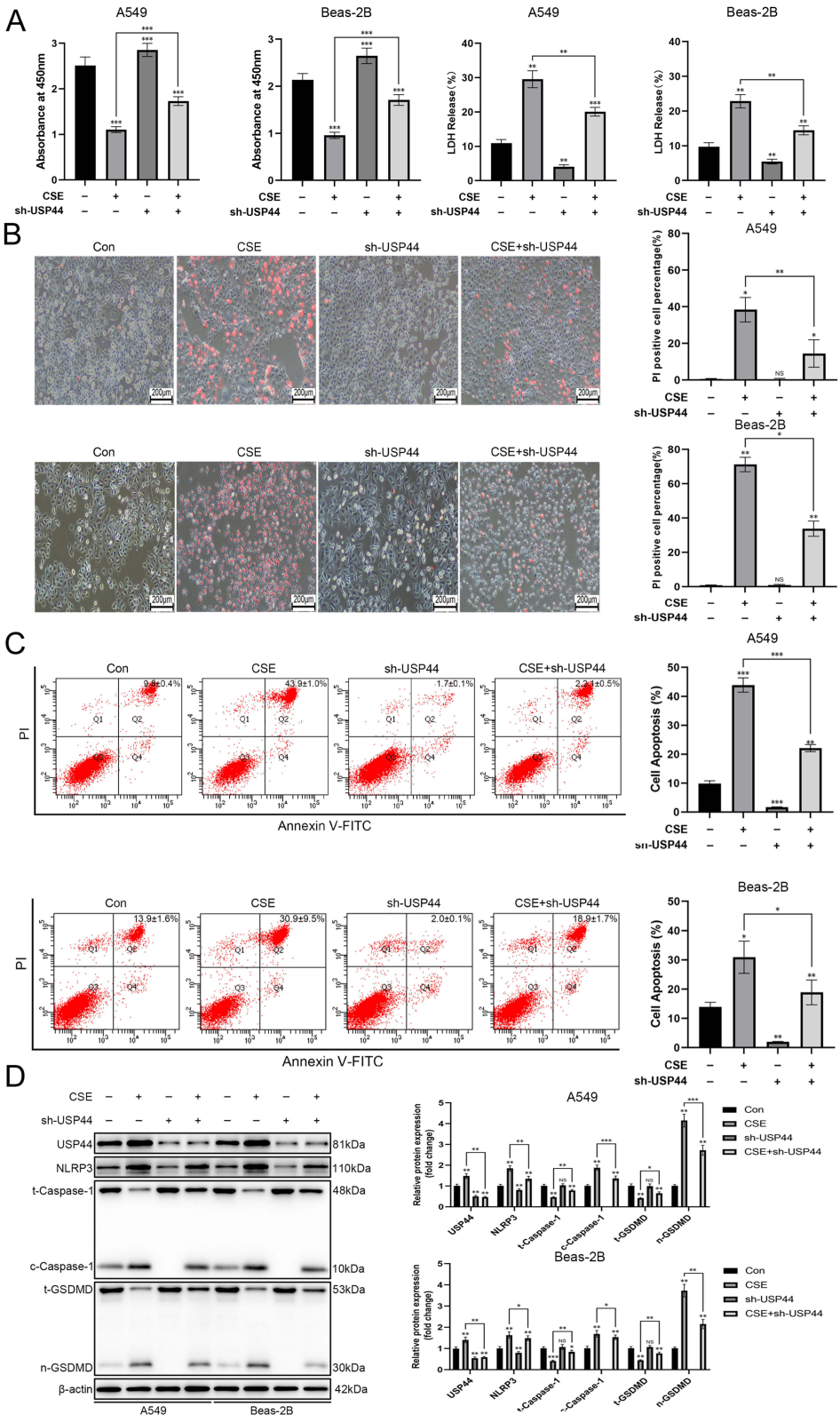

Figure 5 USP44 Knockdown Mitigates CSE-Induced Pyroptosis in Pulmonary Epithelial Cells. (**A**) CCK-8 and LDH assays were employed to evaluate the impact of USP44 knockdown on CSE-induced decreases in cell viability and increases in cell damage levels, respectively; (**B**) The impact of USP44 knockdown on pyroptosis in cells treated with CSE was evaluated using propidium iodide staining; (**C**) The number of pyroptotic cells after USP44 knockdown under CSE induction was measured using flow cytometry; (**D**) Western blot analysis evaluated the expression of NLRP3, Caspase-1, and GSDMD pathway proteins after USP44 knockdown in CSE-treated cells. *$P < 0.05$, **$P < 0.01$, ***$P < 0.001$.

https://doi.org/10.2147/JIR.S546865

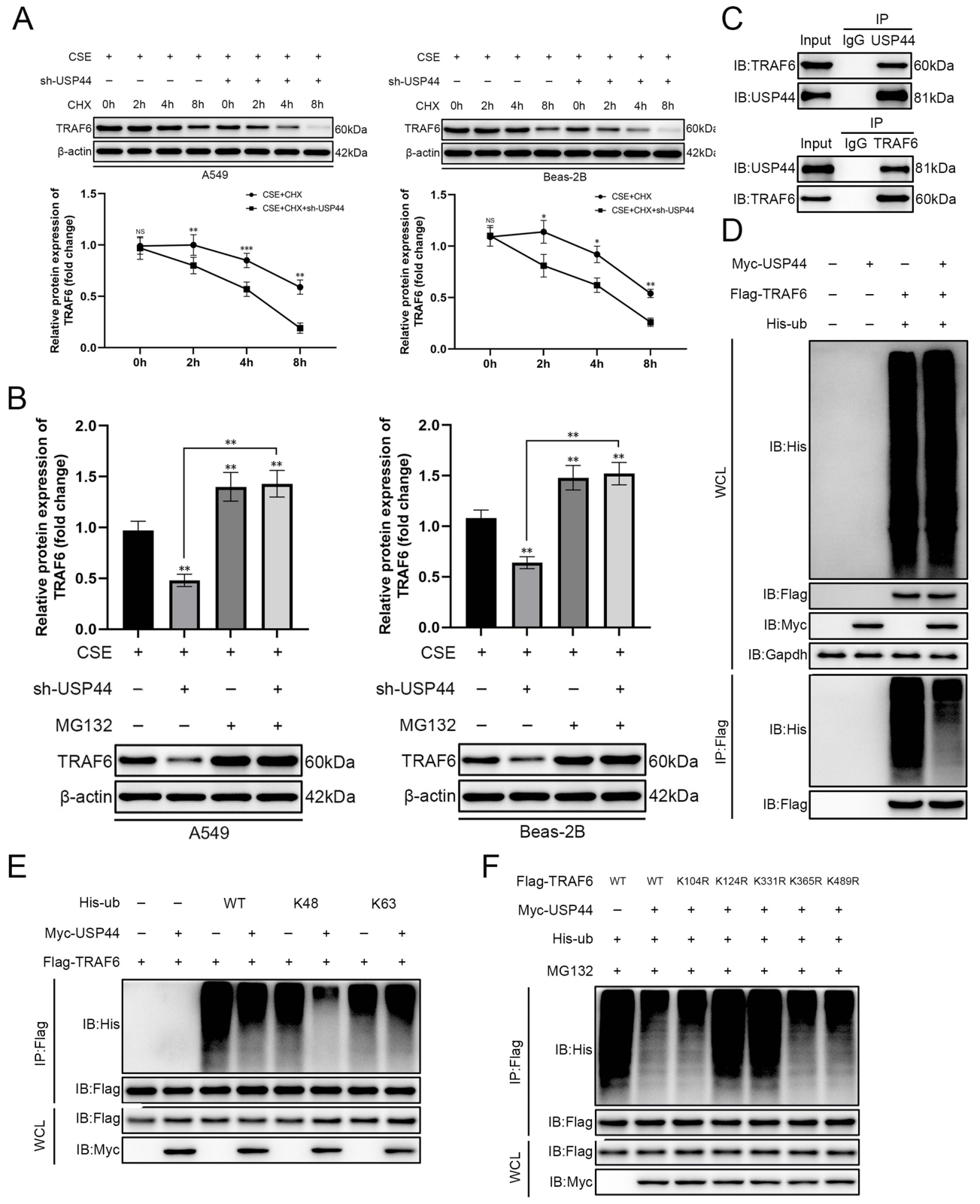

Figure 6 USP44 Augments the Protein Stability of TRAF6. (**A**) CHX assay to assess the impact of USP44 knockdown on the half-life of TRAF6 protein; (**B**) MG132 assay to evaluate the influence of USP44 knockdown on the proteasome-mediated degradation of TRAF6 protein; (**C**) Co-IP experiment to investigate the interaction between USP44 and TRAF6 proteins; (**D**) Ubiquitination IP experiment to analyze the effect of USP44 overexpression on the overall ubiquitination level of TRAF6 protein; (**E**) Ubiquitination IP experiment to determine the type of ubiquitination modification influenced by USP44 overexpression on TRAF6; (**F**) Ubiquitination IP experiment to identify the specific ubiquitination sites on TRAF6 affected by USP44 overexpression. *$P < 0.05$, **$P < 0.01$, ***$P < 0.001$.

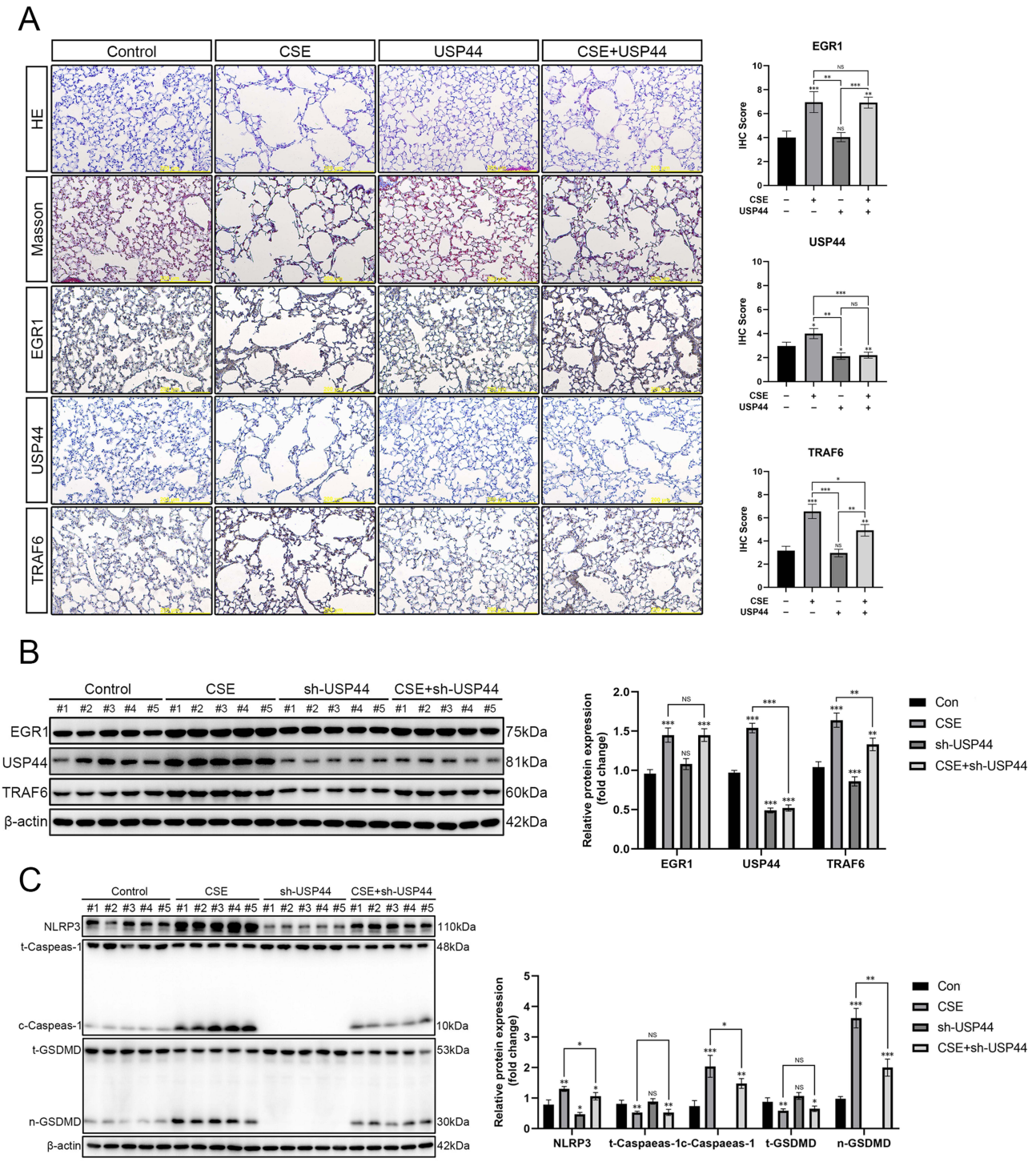

Figure 7 USP44 Knockdown Mitigates Pathological Alterations in a CS-Induced Mouse Model of COPD. (**A**) H&E and Masson staining were employed to evaluate histopathological alterations in the lung tissues of mice exposed to CS, while immunohistochemical staining was conducted to analyze the expression of EGR1, USP44, and TRAF6; (**B**) Changes in the protein levels of EGR1, USP44, and TRAF6 in lung tissues after USP44 knockdown were evaluated using Western blot analysis; (**C**) Western blot analysis was employed to evaluate the expression of NLRP3, Caspase-1, and GSDMD in pulmonary tissues following USP44 knockdown in the CS-induced COPD mouse model.*$P < 0.05$, **$P < 0.01$, ***$P < 0.001$.

tissues, whereas USP44 knockdown markedly diminished TRAF6 expression (Figure 7A and B). Notably, USP44 knockdown alone did not alter baseline pulmonary morphology but specifically attenuated CS-induced pathological changes. We also examined differences in the expression levels of proteins related to the NLRP3/Caspase1/GSDMD signaling pathway in the lung tissues of each group of mice. Western-Blot results showed that CS exposure promoted the

https://doi.org/10.2147/JIR.S546865

expression levels of NLRP3, c-Caspase-1, and n-GSDMD, indicating that CS modeling caused changes in cell pyroptosis. USP44 knockdown significantly attenuated these CS-induced increases, effectively suppressing pyroptosis in vivo (Figure 7C).

Discussion

This study unveils a novel EGR1/USP44/TRAF6 signaling axis through which cigarette smoke promotes pyroptosis in pulmonary epithelial cells, identifying USP44 as the critical deubiquitinating enzyme that executes this regulation, thereby contributing to COPD pathogenesis.

The increasing number of smokers, the rapid aging of the population, and the escalating prevalence of chronic diseases such as diabetes, hypertension, and cardiovascular disorders have resulted in a global prevalence of COPD surpassing 250 million cases, with incidence rates continuing to increase each year.[19] As reported by the World Health Organization (WHO), COPD ranks as the third leading cause of death worldwide, accounting for over 3 million deaths annually.[20] Significantly, more than 90% of deaths attributable to COPD occur in low- and middle-income countries, where diagnostic and therapeutic resources are inadequate. COPD has consequently emerged as a significant public health issue. Currently, no definitive cure exists for COPD. Current therapeutic approaches are primarily limited to pharmacological treatments and lifestyle alterations. Although appropriate pharmacological intervention can reduce the risk of hospitalization and mortality, treatments with bronchodilators, corticosteroids, and antibiotics only delay disease progression without achieving effective disease control.[21] Consequently, there is an urgent need to improve our understanding of COPD pathogenesis and identify novel therapeutic targets.[22]

Smoking is the predominant risk factor for COPD, accounting for roughly 46% of global cases.[23,24] In COPD management, smoking cessation is considered the most effective intervention for preventing or delaying disease progression.[25] Chronic smoking induces oxidative stress in airway epithelial cells, impairs barrier function, increases the release of inflammatory cytokines, and leads to abnormal immune cell recruitment. These processes lead to airway remodeling and structural damage to alveoli, ultimately contributing to the development of emphysema and COPD.[26,27] ER stress is acknowledged as an initial pathological occurrence subsequent to CS exposure. Disruption of ER homeostasis leads to the accumulation of misfolded proteins, consequently activating the unfolded protein response (UPR) to rectify folding defects and preserve cellular function. ER stress entails activation of the PERK/eIF2α/ATF4 signaling cascade. If left unresolved, chronic ER stress can trigger types of programmed cell death, such as apoptosis and ferroptosis.[28] ER stress has been associated with the pathogenesis of COPD.[29] Our experimental data indicated that CSE exposure induces ER stress in pulmonary epithelial cells, activates the PERK/eIF2α/ATF4 signaling pathway, and enhances the expression of the transcription factor EGR1. Knockdown of EGR1 using specific shRNA effectively attenuated CSE-induced lung epithelial cell damage.

The GSDM protein family executes pyroptosis, a form of programmed cell death characterized by the release of pro-inflammatory cytokines such as IL-1β and IL-18.[30] Pyroptosis is considered a "double-edged sword": it contributes to pathogen clearance and the maintenance of tissue homeostasis, whereas excessive pyroptosis can exacerbate inflammatory responses and aggravate disease progression. Accumulating evidence underscores the critical role of pyroptosis in the pathogenesis of inflammatory respiratory diseases.[31] Certain studies indicate that CSE activates the NLRP3/caspase-1/GSDMD pathway in bronchial epithelial cells (BECs), resulting in BEC barrier impairment and lung injury, thereby facilitating the progression of COPD.[32] CSE exposure also induces the generation of abundant reactive oxygen species (ROS), which can cause ER stress and mitochondrial dysfunction. ER stress subsequently activates the PERK/eIF2α/CHOP pathway, leading to upregulated TXNIP, which then activates the NLRP3 inflammasome, thereby inducing pyroptosis.[33] Furthermore, heightened expression of TRAF6 is an additional outcome of CSE exposure. TRAF6 overexpression activates the NLRP3 inflammasome and thereby induces pyroptosis, which is consistent with our findings.[34]

Given the critical role of TRAF6 in promoting pyroptosis, we investigated the upstream mechanisms governing its protein stability. Disruptions in protein homeostasis are closely linked to the pathogenesis of COPD, which exacerbates chronic inflammation, oxidative stress, and apoptosis.[35] The interaction between ubiquitinating and deubiquitinating enzymes is essential for sustaining protein homeostasis.[36] Ubiquitinating enzymes label proteins for degradation, whereas deubiquitinating enzymes eliminate these labels, thereby stabilizing the proteins. A critical function of this regulatory

system is the modulation of inflammatory responses.[37] Our experiments demonstrated that CSE exposure disrupts proteostasis, and that USP44 plays a critical role in this pathology, as its knockdown specifically attenuated CSE-induced damage without affecting basal cellular homeostasis. Numerous studies have demonstrated the role of USP family proteins in the pathogenesis of COPD by regulating proteostasis. In BEAS-2B cells, CSE downregulates the USP25/HDAC11 axis, thereby impairing host defense against Pseudomonas aeruginosa infection in the airways of smokers.[38] CSE exposure downregulates USP49 expression, consequently impairing cell viability in BEAS-2B cells.[39] CSE induces senescence in endothelial progenitor cells (EPCs) by upregulating USP7, which in turn activates the p300-p53/p21 pathway.[40] These findings indicate that targeting ubiquitination or deubiquitination pathways may provide promising therapeutic options for COPD treatment.

This study has several limitations. First, the conclusions are primarily derived from cell lines and murine models without validation in clinical samples or primary human airway epithelial cells. Furthermore, although the sample size of the animal study meets the standards in this field, it may still limit the generalizability of the findings. Second, the research focused on CS-induced COPD and did not examine other pollutants such as biomass smoke or particulate matter. Finally, while we elucidated USP44's role, broader ubiquitination-related networks remain unexplored. These limitations highlight future directions, including employing organoid models to better recapitulate in vivo conditions for COPD pathogenesis research.

Conclusion

This study is the first to unravel the following mechanism in a CS-induced COPD model. CS exposure induces ER stress in pulmonary epithelial cells. This stress activates the PERK/eIF2α/ATF4 signaling pathway. Subsequently, the activation of this pathway leads to the enhanced expression of EGR1. USP44, recognized as a downstream target gene of EGR1, facilitates the stabilization of TRAF6 by orchestrating its deubiquitination at various lysine residues. This stabilization subsequently activates the NLRP3/caspase-1/GSDMD signaling pathway, resulting in pathological pyroptosis and contributing to the pathogenesis of COPD. Therefore, therapeutic strategies aimed at inhibiting EGR1 activation or USP44-mediated deubiquitination could offer a novel and precise intervention for smoke-induced COPD by suppressing dysregulated pyroptosis.

Abbreviations

ATF4, activation transcription factor 4; BECs, bronchial epithelial cells; CCK-8, cell counting kit-8; ChIP, chromatin immunoprecipitation; ChIP-qPCR, chIP coupled with quantitative polymerase chain reaction; COPD, chronic obstructive pulmonary disease; CS, cigarette smoke; CSE, cigarette smoke extract; c-Caspase1, cleaved caspase-1; CHX, cycloheximide; Co-IP, co-immunoprecipitation; DEGs, differentially expressed genes; DMEM, Dulbecco's modified eagle medium; ELISA, Enzyme-Linked Immunoassay; EPD, eukaryotic promoter database; EGR1, early growth response 1; eIF2α, eukaryotic translation initiation factor 2α; ER, endoplasmic reticulum; EPCs, endothelial progenitor cells; GSDMD, gasdermin d; IL-1β, interleukin-1 beta; IL-18, interleukin-18; LDH, lactate dehydrogenase; NLRP3, NOD-like receptor pyrin domain containing 3; n-GSDMD, n-terminal fragment of GSDMD; PERK, PKR-like endoplasmic reticulum kinase; PI, propidium iodide; ROS, reactive oxygen species; SD, standard deviation; TLRs, Toll-like receptors; TRAF6, TNF receptor-associated factor 6; UPR, unfolded protein response; USP44, ubiquitin-specific peptidase 44; WHO, the World Health Organization.

Data Sharing Statement

The datasets used or analyzed during the current study are available from the corresponding author upon reasonable request.

Ethical Approval

This study was approved by the Ethics Committee of the Cancer Hospital of China Medical University (Approval No. GZR202403118). All experimental procedures were conducted in strict accordance with the National Institutes of Health Guide for the Care and Use of Laboratory Animals (NIH Publication No. 8023, revised 1978). This study was carried out

in compliance with the ARRIVE guidelines (Animal Research: Reporting of In Vivo Experiments) and the 3R principles (Replacement, Reduction, Refinement).

Author Contributions

All authors made a significant contribution to the work reported, whether that is in the conception, study design, execution, acquisition of data, analysis and interpretation, or in all these areas; took part in drafting, revising or critically reviewing the article; gave final approval of the version to be published; have agreed on the journal to which the article has been submitted; and agree to be accountable for all aspects of the work.

Funding

This study was supported by the National Natural Science Foundation of China (82072008); the Joint Research Fund of Liaoning Provincial Natural Science Foundation (2023-MSLH-301); the Scientific Research Platform Program of Liaoning Provincial Department of Education (LJ232410164021); the Independent Research Project of Liaoning Provincial Department of Education (LJ212410164020); the Basic Scientific Research Project of Liaoning Provincial Department of Education (JYTMS20231385); and the Scientific Research Project of Shenyang Municipal Health Commission (202316).

Disclosure

All authors declare no competing financial or non-financial interests. The funders had no role in any aspect of this research.

References

1. Upadhyay P, Wu C-W, Pham A, et al. Animal models and mechanisms of tobacco smoke-induced chronic obstructive pulmonary disease (COPD). *J Toxicol Environ Health B Crit Rev*. 2023;26(5):275–305. doi:10.1080/10937404.2023.2208886
2. Celli B, Fabbri L, Criner G, et al. Definition and nomenclature of chronic obstructive pulmonary disease: time for its revision. *Am J Respir Crit Care Med*. 2022;206(11):1317–1325. doi:10.1164/rccm.202204-0671PP
3. Snoderly HT, Alkhadrawi H, Panchal DM, et al. Short-term exposure of female balb/cj mice to e-cigarette aerosol promotes neutrophil recruitment and enhances neutrophil-platelet aggregation in pulmonary microvasculature. *J Toxicol Environ Health B Crit Rev*. 2023;86(8):246–262. doi:10.1080/15287394.2023.2184738
4. Tanner L, Single A. Animal models reflecting chronic obstructive pulmonary disease and related respiratory disorders: translating pre-clinical data into clinical relevance. *J Innate Immun*. 2019;12(3):203–225. doi:10.1159/000502489
5. Qiu S, Sun Q-X, Zhou J, et al. IL-27 mediates anti-inflammatory effect in cigarette smoke induced emphysema by negatively regulating IFN-γ producing cytotoxic $CD8^{+}$T cells in mice. *Eur J Immunol*. 2021;52(2):222–236. doi:10.1002/eji.202049076
6. Zhou L, Jian T, Wan Y, et al. Luteolin alleviates oxidative stress in chronic obstructive pulmonary disease induced by cigarette smoke via modulation of the TRPV1 and CYP2A13/NRF2 signaling pathways. *Int J Mol Sci*. 2023;25(1):369. doi:10.3390/ijms25010369
7. Luo L, Zeng Z, Li T, et al. TET2 stabilized by deubiquitinase USP21 ameliorates cigarette smoke-induced apoptosis in airway epithelial cells. *Iscience*. 2024;27(3):109252. doi:10.1016/j.isci.2024.109252
8. Chung C, Park SY, Huh J-Y, et al. Fine particulate matter aggravates smoking induced lung injury via nlrp3/caspase-1 pathway in COPD. *J Inflamm*. 2024;21(1):13. doi:10.1186/s12950-024-00384-z
9. Zhang M-Y, Jiang Y-X, Yang Y-C, et al. Cigarette smoke extract induces pyroptosis in human bronchial epithelial cells through the ROS/NLRP3/caspase-1 pathway. *Life Sci*. 2021;269:119090. doi:10.1016/j.lfs.2021.119090
10. Zeng Q, Ye L, Ling M, et al. TLR4/TRAF6/NOX2 signaling pathway is involved in ventilation-induced lung injury via endoplasmic reticulum stress in murine model. *Int Immunopharmacol*. 2021;96:107774. doi:10.1016/j.intimp.2021.107774
11. Yang C, Yang C, Huang Z, et al. Reduced expression of mir-125a-5p aggravates lps-induced experimental acute kidney injury pathology by targeting TRAF6. *Life Sci*. 2021;288:119657. doi:10.1016/j.lfs.2021.119657
12. Sun B, Chen Z, Chi Q, Zhang Y, Gao B. Endogenous trna-derived small RNA (tRF3-Thr-AGT) inhibits zbp1/nlrp3 pathway-mediated cell pyroptosis to attenuate acute pancreatitis (AP). *J Cell Mol Med*. 2021;25(22):10441–10453. doi:10.1111/jcmm.16972
13. Cai H, Li H, Xiao X, et al. TRAF6 promotes abdominal aortic aneurysm development by activating macrophage pyroptosis via the NLRP3/Caspase1/GSDMD pathway. *FASEB J*. 2025;3(2):e70318. doi:10.1096/fj.202402873R
14. Liu F, Chen J, Li K, et al. Ubiquitination and deubiquitination in cancer: from mechanisms to novel therapeutic approaches. *Mol Cancer*. 2024;23(1):248. doi:10.1186/s12943-024-02046-3
15. Stintzing S, Lenz H-J. Molecular pathways: turning proteasomal protein degradation into a unique treatment approach. *Clin Cancer Res*. 2014;20(12):3064–3070. doi:10.1158/1078-0432.CCR-13-3175
16. Xia P, Marjan M, Liu Z, et al. Chrysophanol postconditioning attenuated cerebral ischemia-reperfusion injury induced nlrp3-related pyroptosis in a TRAF6-dependent manner. *Exp Neurol*. 2022;357:114197. doi:10.1016/j.expneurol.2022.114197
17. Zou K, Zeng ZG. Role of early growth response 1 in inflammation-associated lung diseases. *Am J Physiol Lung Cell Mol Physiol*. 2023;325(2):L143–L154. doi:10.1152/ajplung.00413.2022

18. Kim D, Ban KY, Lee GH, Jun HS. Lysophosphatidic acid induces podocyte pyroptosis in diabetic nephropathy by an increase of Egr1 expression via downregulation of EzH2. *Int J Mol Sci*. 2023;24(12):9968. doi:10.3390/ijms24129968
19. Duffy SP, Criner GJ. Chronic obstructive pulmonary disease: evaluation and Management. *Med Clin N Am*. 2019;103:453–461. doi:10.1016/j.mcna.2018.12.005
20. World Health Organization. Chronic obstructive pulmonary disease (COPD); 2025. Available from: https://www.who.int/news-room/fact-sheets/detail/chronic-obstructive-pulmonary-disease-(copd). Accessed November 24, 2025.
21. Ammous O, Kampo R, Wollsching-Strobel M, et al. Adherence-enhancing interventions for pharmacological and oxygen therapy in patients with copd: a systematic review and component network meta-analyses. *Eur Respir Rev*. 2024;33(173):240011. doi:10.1183/16000617.0011-2024
22. Liu S, Tan X, Liu S. The role of extracellular vesicles in COPD and potential clinical value. *Respir Res*. 2024;25(1):84. doi:10.1186/s12931-024-02719-z
23. Safiri S, Carson-Chahhoud K, Noori M, et al. Burden of chronic obstructive pulmonary disease and its attributable risk factors in 204 countries and territories, 1990-2019: results from the global burden of disease study 2019. *BMJ*. 2022;378:e069679. doi:10.1136/bmj-2021-069679
24. Burney P, Patel J, Minelli C, et al. Prevalence and population-attributable risk for chronic airflow obstruction in a large multinational study. *Am J Respir Crit Care Med*. 2021;203(11):1353–1365. doi:10.1164/rccm.202005-1990OC
25. Feng L, Lv X, Wang Y, et al. Developments in smoking cessation interventions for patients with chronic obstructive pulmonary disease in the past 5 years: a scoping review. *Expert Rev Respir Med*. 2022;16(7):749–764. doi:10.1080/17476348.2022.2108797
26. Dang X, He B, Ning Q, et al. Alantolactone suppresses inflammation, apoptosis and oxidative stress in cigarette smoke-induced human bronchial epithelial cells through activation of nrf2/ho-1 and inhibition of the nf-κb pathways. *Respir Res*. 2020;21(1):95. doi:10.1186/s12931-020-01358-4
27. Tatsuta M, Kan-o K, Ishii Y, et al. Effects of cigarette smoke on barrier function and tight junction proteins in the bronchial epithelium: protective role of cathelicidin ll-37. *Respir Res*. 2019;20(1):251. doi:10.1186/s12931-019-1226-4
28. Chang C, He F, Ao M, et al. Inhibition of nur77 expression and translocation by compound b6 reduces er stress and alleviates cigarette smoke-induced inflammation and injury in bronchial epithelial cells. *Front Pharmacol*. 2023;14:1200110. doi:10.3389/fphar.2023.1200110
29. Ito H, Yamashita Y, Tanaka T, et al. Cigarette smoke induces endoplasmic reticulum stress and suppresses efferocytosis through the activation of RhoA. *Sci Rep*. 2020;10(1):12620. doi:10.1038/s41598-020-69610-x
30. Frank D, Vince JE. Pyroptosis versus necroptosis: similarities, differences, and crosstalk. *Cell Death Differ*. 2018;26(1):99–114. doi:10.1038/s41418-018-0212-6
31. Song D, Li M, Yu X, et al. The molecular pathways of pyroptosis in atherosclerosis. *Front Cell Dev Biol*. 2022;10:824165. doi:10.3389/fcell.2022.824165
32. Wang L, Meng J, Wang C, Wang Y, Yang C, Li Y. Hydrogen sulfide attenuates cigarette smoke-induced pyroptosis through the tlr4/nf-κb signaling pathway. *Int J Mol Med*. 2022;49(5):56. doi:10.3892/ijmm.2022.5112
33. Mahalanobish S, Dutta S, Saha S, Sil PC. Melatonin induced suppression of er stress and mitochondrial dysfunction inhibited NLRP3 inflammasome activation in COPD mice. *Food Chem Toxicol*. 2020;144:111588. doi:10.1016/j.fct.2020.111588
34. Yang F, Qin H, Qin C, et al. SIRT1 regulates cigarette smoke extract-induced alveolar macrophage polarization and inflammation by inhibiting the TRAF6/NLRP3 signaling pathway. *Mol Med Rep*. 2025;31(2):43. doi:10.3892/mmr.2024.13408
35. Min T, Bodas M, Mazur S, Vij N. Critical role of proteostasis-imbalance in pathogenesis of COPD and severe emphysema. *J Mol Med*. 2011;89(6):577–593. doi:10.1007/s00109-011-0732-8
36. Beck DB, Werner A, Kastner DL, Aksentijevich I. Disorders of ubiquitylation: unchained inflammation. *Nat Rev Rheumatol*. 2022;18(8):435–447. doi:10.1038/s41584-022-00778-4
37. Lopez-Castejon G. Control of the inflammasome by the ubiquitin system. *FEBS J*. 2019;287:11–26. doi:10.1111/febs.15118
38. Long C, Lai Y, Li T, Nyunoya T, Zou C. Cigarette smoke extract modulates Pseudomonas aeruginosa bacterial load via USP25/HDAC11 axis in lung epithelial cells. *Am J Physiol Lung Cell Mol Physiol*. 2020;318(2):L252–L263. doi:10.1152/ajplung.00142.2019
39. Zhang Q, Song W, Ayidaerhan N, He Z. PTPLAD2 and USP49 involved in the pathogenesis of smoke-induced COPD by integrative bioinformatics analysis. *Int J Chron Obstruct Pulmon Dis*. 2020;15:2515–2526. doi:10.2147/COPD.S250576
40. Zeng M, Zhang X, Xing W, Wang Q, Liang G, He Z. Cigarette smoke extract mediates cell premature senescence in chronic obstructive pulmonary disease patients by up-regulating USP7 to activate p300-p53/p21 pathway. *Toxicol Lett*. 2022;359:31–45. doi:10.1016/j.toxlet.2022.01.017